Computer-Aided Design 43 (2011) 1322–1329

Contents lists available at SciVerse ScienceDirect

Computer-Aided Design

journal homepage: www.elsevier.com/locate/cad

C^2 splines covering polar configurations

Ashish Myles [a,*], Jörg Peters [b]

[a] CS Department, New York University, 715 Broadway, 12th Floor, New York, NY 10003, USA

[b] CISE Department, Bldg 42, Rm E301, University of Florida, Gainesville, FL 32611, USA

ARTICLE INFO

Keywords:
C^2
Polar
Spline
B-spline
Curvature-continuous

ABSTRACT

A *polar configuration* is a triangle fan in a quad-dominant mesh; it allows for many mesh lines to join at a single polar vertex. This paper shows how a single tensor-product spline of degree (3, 6) can cap a polar configuration with a C^2 surface. By design, this C^2 polar spline joins C^2 with surrounding bi-3 tensor-product splines and thereby complements algorithms that smoothly cap star-like, multi-sided regions.

1. Motivation

CAD modeling systems represent parametric surfaces by a finite number of quadrilateral spline patches in tensor-product B-spline form. To generate surfaces of arbitrary genus in this representation, a number of algorithms have been devised that smoothly complete a piecewise bicubic C^2 surface, by filling-in star-like, multi-sided holes with n patches as in Fig. 1. But, as pointed out for example in [1], these constructions are not well-suited for high-valence neighborhoods arising from extruded, high-valent or periodic features as in Figs. 2 and 11. Where many patches come together, it is more natural to have a triangle fan join many parameter lines at a common *pole* similar to the latitude/longitude connectivity at the poles of the earth. If such a polar multi-sided hole is to be covered by subdivision, [2] gives simple rules that create a C^2 completion of degree 3. But, except for display, subdivision algorithms do not readily fit into the major CAD modeling frameworks. We therefore develop a new C^2 Polar Spline that, for a polar configuration,

- consists of one tensor-product spline of degree (3, 6),
- is easy to construct, by formulas (4)–(6) of Section 6,
- is easy to analyze, and
- is *bi*-3 C^2 *compatible*, that is, meets C^2 with surrounding C^2 bi-3 tensor-product splines.

In more detail, the C^2 Polar Spline is of degree 6 in the periodic direction and of degree 3 in the radial direction. One boundary is collapsed to a single point $\mathbf{p}_0$, the pole (cf. Figs. 3 and 6(c)). Since the spline is C^2, the degree 6 periodic direction has 4-fold knots. The knots in the radial direction are repeated so that $\mathbf{p}_0$ is interpolated. The spline is derived by explicitly relating its control points to a second-order expansion of the surface at the pole in a special shape basis.

Overview. After reviewing related literature, formally stating the challenge, pointing to observations that enable the construction and laying out the tools (Sections 2–5), we formally state the algorithm in Section 6. Section 7 proves curvature continuity and bi-3 C^2 compatibility of C^2 polar splines. Section 8 explains what alternative constructions are possible and why we chose the particular set of rules. Section 9 explores the relation of polar splines to polar subdivision. Section 10 concludes with a gallery of shapes and its discussion.

2. Related work

A number of constructions yield curvature-continuous free-form surfaces from coarse control meshes, for example [3,6–10,4,5]. Techniques that generate C^2 spline surfaces on arbitrary quad meshes include Prautzsch's free-form splines [3] and Reif's TURBS [6], both of degree bi-6; Karčiauskas and Peters' guided spline surfaces [10,4]; and Loop and Schaefers' bi-7 construction [5], improving [11]. Ying and Zorin's approach [8] generates surfaces from quad meshes by joining locally-defined polynomials via exponential blending functions. Bohl and Reif [12] use a careful reparameterization to analyze constructions with multiple collapsed layers of control points. All the above constructions represent parametric surfaces by a finite number of patches.

Quad-based subdivision algorithms, while enabling free-form modeling with simple implementations, do not readily fit into this framework. And it has proven difficult to generate C^2 surfaces based on subdivision for star-like configurations. Levin [9] blended Catmull–Clark subdivision surfaces near extraordinary vertices with polynomials to produce curvature continuity at extraordinary points. For triangle meshes, Zorin [13] similarly blended Loop subdivision surfaces with polynomials, but used blending functions that were themselves subdivision surfaces. At present, we are unaware of any *simple* subdivision algorithms for covering star-like holes by a C^2 surface cap.

* Corresponding author. Tel.: +1 212 998 3319.
E-mail addresses: amyles@cs.nyu.edu, marcianx@gmail.com (A. Myles), jorg@cise.ufl.edu (J. Peters).

0010-4485/$ – see front matter © 2011 Elsevier Ltd. All rights reserved.
doi:10.1016/j.cad.2011.08.018

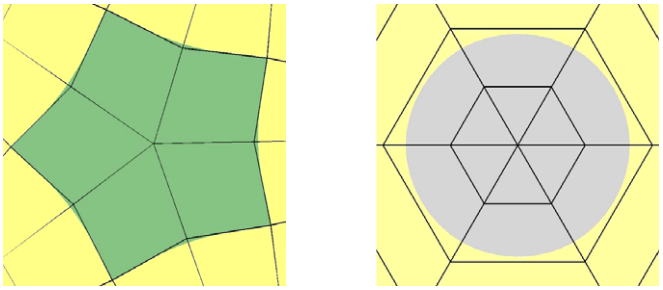

(a) Star-like layout. (b) Polar layout.

Fig. 1. (a) A star-like mesh-configuration covered by n patches. (b) A polar configuration covered by one polar spline.

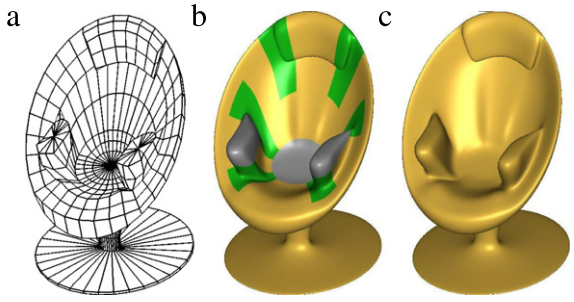

Fig. 2. Polar Chair. (a) A mesh with three polar configurations (arm-rests,center), as well as star-like (Catmull–Clark-type) extraordinary vertices, defines a smooth manifold (c) consisting of a small number of tensor-product splines. (b) Uniform bi-3 splines are *gold*, C^2 polar splines are *gray*; star-like-neighborhoods can be covered by, for example, by one of [3–5] (*green*). (For interpretation of the references to colour in this figure legend, the reader is referred to the web version of this article.)

For polar configurations, Karčiauskas et al. [14] defined a C^2 surface consisting of an infinite sequence of surface rings of degree (5, 6) and Myles and Peters improved on this with a bi-3 C^2 subdivision construction with simple rules [2]. The corresponding limit surface consists of an infinite sequence of polynomial surface rings. The C^2 polar splines constructed below provide a finite CAD-friendly counterpart to this algorithm. Another finite construction, with n Bézier patches of degree (6,5) appeared in [15]. This pairing of subdivision with a finite patch construction is analogous to pairing bi-3 polar subdivision with a bi-3 spline C^1 construction in [16]. (Section 9 describes an alternative bi-3 spline derived from the new framework that has fewer control points.)

3. Polar configurations and C^2 expansions

A *k-layer* **polar configuration** is a submesh consisting of a triangle fan surrounded by k layers of quads that have only 4-valent vertices (see Fig. 6(a)). The central vertex of the triangle fan is the *polar vertex*, and its valence is denoted n. The corresponding point on the spline surface is the *pole*. A designer can easily separate a polar vertex from another polar vertex or a star-like configuration by adding an edge loop encircling the polar vertex.

Table 1
The shape basis. Our choice (4) of v and change of parameterization from (b)→(c) produce the shape basis(c). When converted to polar coordinates (d), each basis in function (c) belongs to exactly one Fourier frequency (e).

k	$h_{w_k}(r,\gamma)$	Reparam.	Polar coord.	θ freq.
0	1	1	1	0
1	$rf_{v_1}(\gamma)$	x	$\rho\cos(\theta)$	1
2	$rf_{v_2}(\gamma)$	y	$\rho\sin(\theta)$	1
3	$r^2(f^2_{v_1}(\gamma)+f^2_{v_2}(\gamma))$	x^2+y^2	ρ^2	0
4	$r^2(f^2_{v_1}(\gamma)-f^2_{v_2}(\gamma))$	x^2-y^2	$\rho^2\cos(2\theta)$	2
5	$r^2(2f_{v_1}(\gamma)f_{v_2}(\gamma))$	$2xy$	$\rho^2\sin(2\theta)$	2
(a)	(b)	(c)	(d)	(e)

Two layers of control points in the vicinity of the polar vertex will determine the second-order expansion of the surface at the pole. The control points will be linearly combined to create control points in the following *shape basis* of polynomials of order 2:

$$\mathbf{s} := [1, x, y, x^2+y^2, x^2-y^2, 2xy]. \tag{1}$$

The shape basis is similar both to the power-form expansion and to the expansion in polar coordinates $(x, y) = (\rho\cos(\theta), \rho\sin(\theta))$. Table 1(c, d) shows how each basis function in $\mathbf{s}$ corresponds to exactly one θ frequency. Thus, defining a quadratic surface as

$$\mathbf{p}_0 + \mathbf{p}_1 x + \mathbf{p}_2 y + \mathbf{p}_3(x^2+y^2) + \mathbf{p}_4(x^2-y^2) + \mathbf{p}_5(2xy) \tag{2}$$

gives $\mathbf{p}_0, \mathbf{p}_1, \mathbf{p}_2, \mathbf{p}_3, \mathbf{p}_4, \mathbf{p}_5 \in \mathbb{R}^3$ the intuitive geometric meaning illustrated in Fig. 3:

- $\mathbf{p}_0$ is a point on the surface;
- $\mathbf{p}_1$ and $\mathbf{p}_2$ help span the tangent plane;
- $\mathbf{p}_3$ determines the ellipticity; and
- $\mathbf{p}_4$ and $\mathbf{p}_5$ together define the orientation and magnitude of the saddle components.

4. Observations that enable the construction

First, consider a quad mesh with polar configurations converted to bi-3 splines except for surface 'caps' defined by star-like and polar configurations. Fig. 1 illustrates how a corresponding polar

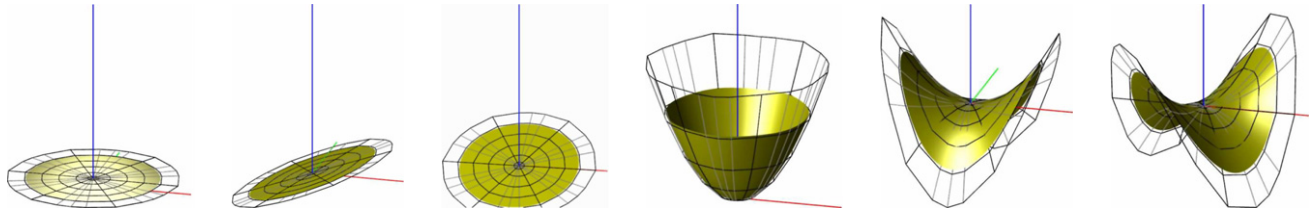

(a) 1. (b) x. (c) y. (d) x^2+y^2. (e) x^2-y^2. (f) $2xy$.

Fig. 3. The shape basis represents geometric properties of the surface: (a) position, (b and c) tangent plane, (d) elliptic, and (e and f) hyperbolic expansion terms. The control nets are defined by (16).

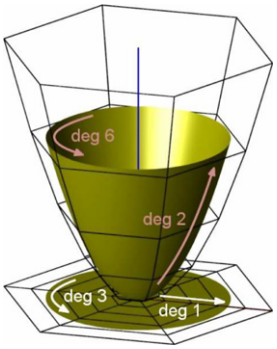

Fig. 4. C^2 polar splines require degree (2, 6) to represent graphs of quadratics.

cap is surrounded by a single smooth curve while the star-like cap's boundary is a zigzag curve. Correspondingly, the polar cap can be a single, parametrically C^2, periodic spline patch whose outer boundary matches the boundary of the polar configuration; while star-like caps consist naturally of n patches with distinct parameterization that may be joined with geometric, namely G^2 continuity.

Secondly, we can approximate the disk $(\rho\cos(\theta), \rho\sin(\theta))$, $\rho \in [0 \ldots 1]$, $\theta \in [0 \ldots 2\pi]$ by a C^2 periodic polynomial spline $(u, v) \to (x, y)$ that is of degree 1 in the *radial direction* emanating from the polar vertex and of degree 3 in the *periodic direction* approximating sine and cosine variation. No less than degree 3 will do if we require parametric C^2 continuity in the periodic direction. Consequently, the space of quadratic functions $z(x, y)$ includes maps of degree $(2, 6)$ in the spline parameters. This is illustrated in Fig. 4 and was also shown in [2].

Finally, as displayed in Table 1(d), each function in the basis $\mathbf{s}$ can be viewed as a radial function tensored with a periodic function. Section 5 gives a specific choice of univariate periodic degree 3 splines, $f_{\mathrm{v}_1}(\gamma)$ and $f_{\mathrm{v}_2}(\gamma)$, that approximate $\cos(2\pi\gamma/n)$ and $\sin(2\pi\gamma/n)$, respectively. Then parameterizing $(x, y) = (rf_{\mathrm{v}_1}(\gamma), rf_{\mathrm{v}_2}(\gamma))$ yields the factored basis functions of degree $(3, 6)$ of $\mathbf{s}$ in Table 1(b) that are suitable for parameterizing the neighborhood of the pole as shown in Fig. 3. (The precise degree to which cosine and sine are approximated is irrelevant for curvature continuity as the proof in Section 7 only relies on the reparameterization above being valid — i.e. a diffeomorphism away from the origin.)

5. C^2 polar spline basics

As illustrated in Fig. 6, we will fit one periodic spline to each polar configuration in the quad mesh. Since we construct the spline independently in each coordinate, we distinguish vectors in $\mathbb{R}^3$ using boldface, e.g. $\mathbf{q}_{ij}, \mathbf{b}_{ij}, \mathbf{p}_k \in \mathbb{R}^3$, from scalars representing one coordinate, using teletype: $\mathrm{q}_{ij}, \mathrm{b}_{ij}, \mathrm{p}_k \in \mathbb{R}$. We want to tensor univariate radial and periodic functions in the bases of Table 1(b). Therefore, in the radial direction, the algorithm will generate the functions $\{1, r, r^2\}$ using cubic splines and, in the periodic direction, the splines

$$(f_{\mathrm{v}_0}, f_{\mathrm{v}_1}, f_{\mathrm{v}_2}, f_{\mathrm{v}_3}, f_{\mathrm{v}_4}, f_{\mathrm{v}_5}) := (1, f_{\overline{\mathrm{v}}_1}, f_{\overline{\mathrm{v}}_2}, f_{\overline{\mathrm{v}}_1}^2 + f_{\overline{\mathrm{v}}_2}^2, f_{\overline{\mathrm{v}}_1}^2 - f_{\overline{\mathrm{v}}_2}^2, 2f_{\overline{\mathrm{v}}_1}f_{\overline{\mathrm{v}}_2}) \quad (3)$$

based on univariate periodic splines $f_{\overline{\mathrm{v}}_1}$ and $f_{\overline{\mathrm{v}}_2}$ of degree 3 that approximate cosine and sine. To define the periodic functions, we use the following notation.

Univariate periodic splines: Let n be the valence of the polar vertex. Let $\mathcal{P}_k$ be the *space of control polygons* of periodic C^2 splines with uniformly-spaced knots of multiplicity $k - 2$ (Fig. 5(a)–(b)). We define a C^2 periodic *spline* of degree d, $d > 2$,

$$f_{\mathrm{a}} : [0, 1] \to \mathbb{R}, \quad \mathrm{a} \in \mathcal{P}_d := \mathbb{R}^{(d-2)n}$$

by uniformly-spaced, $(d - 2)$-fold knots at the integers modulo n scaled down by n, $\frac{1}{n}\mathbb{Z}_n$, and control points a with periodic repetition. That is, for $d = 3$ the knot sequence is just $\frac{1}{n}\mathbb{Z}_n$ and for $d = 6$,

$$\frac{1}{n}[0, 0, 0, 0, 1, 1, 1, 1, \ldots, n{-}1, n{-}1, n{-}1, n{-}1].$$

***i*-link:** We define the *i-link* of a polar configuration $\mathbf{q}$ to be a n-vector of vertices that are i radial edges away from the polar vertex $\mathbf{q}_{i\circ} := [\mathbf{q}_{ij}]_{j\in\mathbb{Z}_n}$ (Fig. 5(c)). The vector $\mathbf{q}_{i\circ}$ can be interpreted as an element of $\mathcal{P}_3$.

Spline multiplication: The operator $\diamond : \mathcal{P}_3 \times \mathcal{P}_3 \to \mathcal{P}_6$ expresses spline multiplication in terms of the control points:

$$f_{\overline{\mathrm{a}}_1} f_{\overline{\mathrm{a}}_2} = f_{\overline{\mathrm{a}}_1 \diamond \overline{\mathrm{a}}_2} \quad \text{for } \overline{\mathrm{a}}_1, \overline{\mathrm{a}}_2 \in \mathcal{P}_3.$$

In particular, if $\mathbf{1} \in \mathcal{P}_3$ is the vector of all 1s, $\overline{\mathrm{a}} \diamond \mathbf{1} \in \mathcal{P}_6$, and $f_{\overline{\mathrm{a}}\diamond\mathbf{1}}$ is the degree-raised representation of $f_{\overline{\mathrm{a}}}$. The Appendix gives explicit formulas and code to implement the $\diamond$ operator. This and weighted vector addition are the only operations needed for implementing C^2 polar splines.

Periodic bases f_{v_k}: Cosine and sine can be approximated by a pair of degree 3 splines $f_{\overline{\mathrm{v}}_1}$ and $f_{\overline{\mathrm{v}}_2}$ with coefficients $\overline{\mathrm{v}}_1, \overline{\mathrm{v}}_2 \in \mathcal{P}_3$,

$$(\overline{\mathrm{v}}_1)_j := \cos\frac{2\pi j}{n} \quad \text{and} \quad (\overline{\mathrm{v}}_2)_j := \sin\frac{2\pi j}{n}.$$

The coefficients v_k of the basis functions f_{v_k} (3) are then computed from $\overline{\mathrm{v}}_1$ and $\overline{\mathrm{v}}_2$ as

$$\begin{aligned} \mathrm{v}_0 &:= \mathbf{1} \diamond \mathbf{1} \in \mathcal{P}_6, & \mathrm{v}_3 &:= \overline{\mathrm{v}}_1 \diamond \overline{\mathrm{v}}_1 + \overline{\mathrm{v}}_2 \diamond \overline{\mathrm{v}}_2, \\ \mathrm{v}_1 &:= \overline{\mathrm{v}}_1 \diamond \mathbf{1}, & \mathrm{v}_4 &:= \overline{\mathrm{v}}_1 \diamond \overline{\mathrm{v}}_1 - \overline{\mathrm{v}}_2 \diamond \overline{\mathrm{v}}_2, \\ \mathrm{v}_2 &:= \overline{\mathrm{v}}_2 \diamond \mathbf{1}, & \mathrm{v}_5 &:= 2\overline{\mathrm{v}}_1 \diamond \overline{\mathrm{v}}_2. \end{aligned} \quad (4)$$

6. C^2 polar spline construction

This section defines the polar spline $h_{\mathbf{b}}(r, \gamma)$ algorithmically. We determine the control points $\mathbf{b}_{ij} \in \mathbb{R}^3$, separately for each x, y or z-coordinate $\mathrm{b}_{ij} \in \mathbb{R}$ as linear expressions in $\mathrm{p}_k\mathrm{v}_k$, $k = 0, \ldots, 5$. Here v_k defines the periodic behavior of the spline, while $\mathrm{p}_k \in \mathbb{R}$ represents the quadratic radial expansion derived from the polar configuration.

Input: a 2-layer polar configuration

Fig. 6(a) shows a 2-layer polar configuration defining the polar cap.

Output: one bivariate periodic spline $h_{\mathbf{b}} \in \mathbf{s}$ Fig. 6(c) labels the coefficients

$$\mathrm{b}_{ij} \in \mathbb{R} \quad \text{for } i \in \{0, 1, \ldots, 6\} \text{ and } j \in \mathbb{Z}_{4n}$$

of one coordinate of the C^2 polar spline. The polar spline is a single tensor-product spline patch $h_{\mathbf{b}}(r, \gamma)$ of degree $(3, 6)$. Its knots are $[0, 0, 0, 0, 1, 2, 3, 4, 5, 6, 7]$ in the radial parameter r and are uniformly-spaced 4-fold knots in the periodic parameter γ.

Algorithm

Step 0. We apply the masks of Appendix B to refine the input 2-layers to a 4-layer polar configuration with $6n$ vertices

$$(\mathbf{q}_{ij})_{i\in\{0,1,\ldots,5\}, j\in\mathbb{Z}_n} \quad (\text{per coordinate: } \mathrm{q}_{ij})$$

that are indexed by i in the radial direction and by j in the periodic direction as shown in Fig. 6(b). The polar vertex $\mathbf{q}_{0j} := \mathbf{q}_{00}$ is replicated n times.

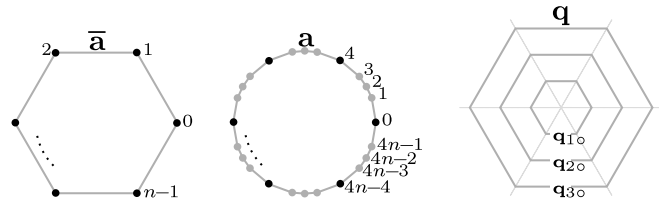

(a) $\bar{a} \in \mathcal{P}_3$. (b) $a \in \mathcal{P}_6$. (c) i-links of $\mathbf{q}$.

Fig. 5. Notation. (a) A periodic control polygon with n coefficients of a degree 3 spline with uniform knots. (b) A periodic control polygon with $4n$ coefficients of a degree 6 spline with 4-fold knots. (c) Periodic i-links of a polar configuration (in thick gray).

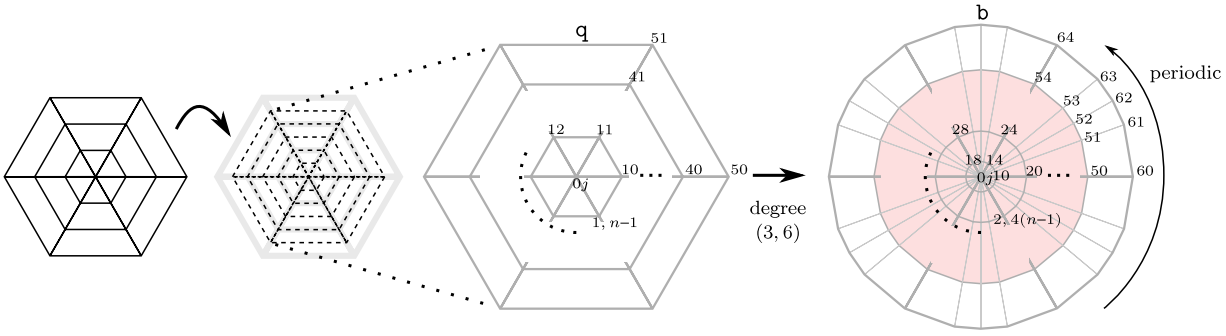

(a) Input. (b) Subdivided input q. (c) Output: spline h_{b}.

Fig. 6. Construction of the C^2 polar spline. (a) A 2-layer polar configuration is once-refined by bicubic polar subdivision [16] to yield (b) the 4-layer configuration q. From q, the construction derives (c) the control points b of the spline h_{b} (*pink*) of degree (3, 6). (For interpretation of the references to colour in this figure legend, the reader is referred to the web version of this article.)

Step 1. Compute $\mathrm{v}_k \in \mathcal{P}_6$ by (4).

Step 2. Let $c_\gamma := \cos(2\pi\gamma)$ and $s_\gamma := \sin(2\pi\gamma)$ and q_{ij} one coordinate of the output from Step 0. Then compute

$$\begin{aligned}
\mathrm{p}_0 &:= \frac{2}{3}\mathrm{q}_{00} + \frac{1}{3n}\sum_{j=0}^{n-1}\mathrm{q}_{1j}, \qquad \mathrm{p}_3 := -\mathrm{q}_{00} + \frac{1}{n}\sum_{j=0}^{n-1}\mathrm{q}_{1j},\\
\mathrm{p}_1 &:= \frac{2}{n}\sum_{j=0}^{n-1} c_{j/n}\mathrm{q}_{1j}, \qquad \mathrm{p}_4 := \frac{2}{n}\sum_{j=0}^{n-1} c_{2j/n}\mathrm{q}_{1j} \in \mathbb{R}\\
\mathrm{p}_2 &:= \frac{2}{n}\sum_{j=0}^{n-1} s_{j/n}\mathrm{q}_{1j}, \qquad \mathrm{p}_5 := \frac{2}{n}\sum_{j=0}^{n-1} s_{2j/n}\mathrm{q}_{1j}.
\end{aligned} \tag{5}$$

Step 3. For each coordinate, form the spline's coefficients

$$\begin{aligned}
\mathrm{b}_{0\circ} &:= \mathrm{p}_0\mathrm{v}_0 \quad \in \mathcal{P}_6\\
\mathrm{b}_{1\circ} &:= \mathrm{p}_0\mathrm{v}_0 + \frac{1}{3}(\mathrm{p}_1\mathrm{v}_1 + \mathrm{p}_2\mathrm{v}_2)\\
\mathrm{b}_{2\circ} &:= \mathrm{p}_0\mathrm{v}_0 + \frac{1}{3}(\mathrm{p}_1\mathrm{v}_1 + \mathrm{p}_2\mathrm{v}_2) + \frac{2}{3}(\mathrm{p}_3\mathrm{v}_3 + \mathrm{p}_4\mathrm{v}_4 + \mathrm{p}_5\mathrm{v}_5)\\
\mathrm{b}_{i\circ} &:= \mathrm{q}_{i-1,\circ} \diamond \mathbf{1} \quad \text{for } i \in \{3, 4, 5, 6\}.
\end{aligned} \tag{6}$$

Since v_0 is a vector of all 1s, $\mathbf{b}_{0\circ}$ is collapsed to the single point $\mathbf{p}_0$ so that the pole is well-defined.

Comments. Step 0 can be omitted if there is no other extraordinary or polar vertex in the 4-link. Then the 4-link can be used directly. The values computed in Step 1 can be pre-computed for a range of n so that the step can be omitted. The choice of p_k in Step 2 is explained in Section 8: p_1, p_2, p_4, and p_5 are computed using the discrete Fourier transform in the periodic direction, while the formulas for p_0 and p_3 emulate cubic B-spline knot-insertion in the radial direction. Step 3 defines the innermost i-links $\mathrm{b}_{0\circ}$, $\mathrm{b}_{1\circ}$, and $\mathrm{b}_{2\circ}$ of the quadratic expansion (2) at the pole. The outer i-links $\mathrm{b}_{3\circ}$, $\mathrm{b}_{4\circ}$, $\mathrm{b}_{5\circ}$, $\mathrm{b}_{6\circ}$, are degree-raised i-links of the polar configuration.

7. Proof of curvature continuity

C^2 continuity between the output spline h_{b} and surrounding bi-3 splines is straightforward since, by (6), the control points $\mathrm{b}_{3\circ}, \ldots, \mathrm{b}_{6\circ}$ define the same surface (in degree-raised form) as $\mathrm{q}_{2\circ}, \ldots, \mathrm{q}_{5\circ}$. Therefore h_{b} is bi-3 C^2 compatible as claimed.

To prove curvature continuity at the pole $h_{\mathrm{b}}(0, 0)$, we derive an explicit expansion at the pole.

Theorem 1. *The polar spline h_{b} is C^2 at the pole.*

Proof. We show that, at $(0, 0)$, the spline $h_{\mathrm{b}}(r, \gamma)$ differs from a quadratic map $\tilde{h}(r, \gamma)$ by $o(r^2)$ in the radial parameter r.

We define $\tilde{h}(r, \gamma)$ as a spline of degree (3, 6):

$$\tilde{h}(r, \gamma) := \sum_{k=0}^{5} \mathrm{p}_k f_{\mathrm{v}_k}(\gamma) g_{\mathrm{u}_k}(r), \tag{7}$$

where p_k is defined by (5), $\mathrm{v}_k \in \mathcal{P}_6$ by (4), f_{v_k} by (3),

$$\begin{aligned}
\mathrm{u}_0 &:= [1, 1, 1, 1, 1, 1, 1],\\
\mathrm{u}_1 &:= \mathrm{u}_2 := \left[0, \frac{1}{3}, 1, 2, 3, 4, 5\right],\\
\mathrm{u}_3 &:= \mathrm{u}_4 := \mathrm{u}_5 := \frac{1}{3}[0, 0, 2, 11, 26, 47, 74],
\end{aligned} \tag{8}$$

and $g_{\mathrm{u}_k}(r)$ is the univariate C^2 degree-3 spline with coefficient vector u_k and knots $[0, 0, 0, 0, 1, 2, 3, 4, 5, 6, 7]$. By this choice of u_k,

$$\begin{aligned}
g_{\mathrm{u}_0}(r) &= 1,\\
g_{\mathrm{u}_1}(r) &= g_{\mathrm{u}_2}(r) = r,\\
g_{\mathrm{u}_3}(r) &= g_{\mathrm{u}_4}(r) = g_{\mathrm{u}_5}(r) = r^2,
\end{aligned} \tag{9}$$

so that $\tilde{h}(r, \gamma)$ represents the quadratic expansion (2) as is evident after the change of variables $(x, y) := (r f_{\bar{\mathrm{v}}_1}(\gamma), r f_{\bar{\mathrm{v}}_2}(\gamma))$ suggested

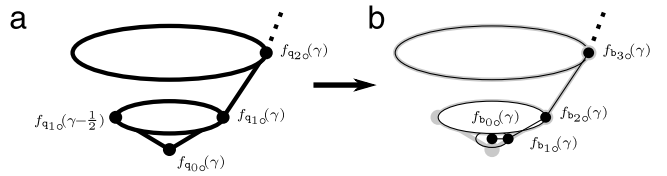

Fig. 7. Knot insertion analogy. The conversion of a symmetric (infinite-valent) polar configuration q to spline control points b corresponds to knot insertion in the radial direction.

in Table 1(b, c):

$$\begin{aligned}\tilde{h}(r,\gamma) &\overset{(9)}{=} \mathrm{p}_0 + r(\mathrm{p}_1 f_{\mathrm{v}_1}(\gamma) + \mathrm{p}_2 f_{\mathrm{v}_2}(\gamma)) \\ &\quad + r^2(\mathrm{p}_3 f_{\mathrm{v}_3}(\gamma) + \mathrm{p}_4 f_{\mathrm{v}_4}(\gamma) + \mathrm{p}_5 f_{\mathrm{v}_5}(\gamma)) \\ &\overset{(4)}{=} \mathrm{p}_0 + r(\mathrm{p}_1 f_{\bar{\mathrm{v}}_1}(\gamma) + \mathrm{p}_2 f_{\bar{\mathrm{v}}_2}(\gamma)) + r^2(\mathrm{p}_3(f_{\bar{\mathrm{v}}_1}(\gamma)^2 + f_{\bar{\mathrm{v}}_2}(\gamma)^2) \\ &\quad + \mathrm{p}_4(f_{\bar{\mathrm{v}}_1}(\gamma)^2 - f_{\bar{\mathrm{v}}_2}(\gamma)^2) + \mathrm{p}_5(2 f_{\bar{\mathrm{v}}_1}(\gamma) f_{\bar{\mathrm{v}}_2}(\gamma))) \\ &= \mathrm{p}_0 + \mathrm{p}_1 x + \mathrm{p}_2 y + \mathrm{p}_3(x^2+y^2) + \mathrm{p}_4(x^2-y^2) + \mathrm{p}_5(2xy).\end{aligned}$$

The first three formulas in (6) may be rewritten as follows.

$$\begin{bmatrix}\mathrm{b}_{0\circ}\\ \mathrm{b}_{1\circ}\\ \mathrm{b}_{2\circ}\end{bmatrix} = \begin{bmatrix}1 & 0 & 0\\ 1 & \frac{1}{3} & 0\\ 1 & 1 & \frac{2}{3}\end{bmatrix}\begin{bmatrix}\mathrm{p}_0\mathrm{v}_0\\ \mathrm{p}_1\mathrm{v}_1+\mathrm{p}_2\mathrm{v}_2\\ \mathrm{p}_3\mathrm{v}_3+\mathrm{p}_4\mathrm{v}_4+\mathrm{p}_5\mathrm{v}_5\end{bmatrix}.$$

Since the columns of the matrix agree with u_k, it is clear that the pole-most three i-links of h_{b} agree with those of $\tilde{h}$. Consequently, $h_{\mathrm{b}}(r,\gamma) = \tilde{h}(r,\gamma) + o(r^2)$ and the quadratic expansion of $\tilde{h}(r,\gamma)$ matches that of $\tilde{h}(r,\gamma)$ at $(0,0)$. □

For generic input data, the polar spline cap with coordinates h_{b} therefore has a C^2 embedding at the pole.

8. Mapping a polar configuration q to the quadratic expansion coefficients p_k

Theorem 1 does not depend on the choice of the six coefficients p_k that define the geometry of the quadratic expansion at pole. Our choice (5) of the p_k represents a natural projection from the polar configuration.

Since each function in **s** corresponds to precisely one Fourier frequency in the periodic direction (cf. Table 1(d)), it is natural to match these frequencies, by having the formulas for p_k, $k \in \{1,2,4,5\}$ match the discrete Fourier transforms of the 1-link $\mathrm{q}_{1\circ}$.

Since the Fourier transform of the 1-link only prescribes an average and does not include a contribution from the polar vertex q_{00}, the formulas for p_0 and p_3 are derived to mimic knot-insertion into a uniform cubic B-spline in the radial direction. To see this, we consider the limit as $n \to \infty$ and interpret the dense set of control points as a function of γ (see Fig. 7). For simplicity, we consider an initial control mesh $\mathrm{q}_{1\circ}$ that is symmetric under rotation about the axis through q_{00} and $\mathrm{avg}_\gamma(\mathrm{q}_{1\gamma})$, the average (centroid) of the dense set of 1-link control points. Then $\mathrm{p}_4 = \mathrm{p}_5 = 0$ and

$$f_{\mathrm{b}_{1\circ}}(\gamma) \overset{(6)}{=} \mathrm{p}_0 + \frac{1}{3}(\mathrm{p}_1 c_\gamma + \mathrm{p}_2 s_\gamma), \tag{10}$$

$$\begin{aligned}f_{\mathrm{b}_{2\circ}}(\gamma) &\overset{(6)}{=} \mathrm{p}_0 + \mathrm{p}_1 c_\gamma + \mathrm{p}_2 s_\gamma + \frac{2}{3}\left(\mathrm{p}_3 + \cancel{\mathrm{p}_4}^{0} c_{2\gamma} + \cancel{\mathrm{p}_5}^{0} s_{2\gamma}\right) \\ &= \mathrm{p}_0 + \mathrm{p}_1 c_\gamma + \mathrm{p}_2 s_\gamma + \frac{2}{3}\mathrm{p}_3.\end{aligned} \tag{11}$$

We now focus on one radial slice with fixed angle γ. Due to density, $f_{\mathrm{q}_{1\circ}}(\gamma - \frac{1}{2})$ is well-defined, we can consider control points $[f_{\mathrm{q}_{1\circ}}(\gamma - \frac{1}{2}), f_{\mathrm{q}_{0\circ}}(\gamma), f_{\mathrm{q}_{1\circ}}(\gamma), f_{\mathrm{q}_{2\circ}}(\gamma), f_{\mathrm{q}_{3\circ}}(\gamma)]$ of a radial cubic spline with knots $[-3,-2,-1,0,1,2,3,4,5]$ (Fig. 7(a)). We define p and hence b by 3-fold knot insertion at 0:

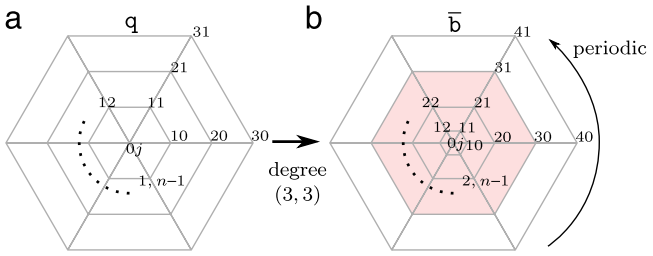

Fig. 8. A C^1 **polar spline.** (a) A 2-layer polar configurationq can be converted without an intermediate subdivision step to (b) a bi-3 spline $h_{\bar{\mathrm{b}}}$ defined by control points $\bar{\mathrm{b}}$ (in the central *pink* region). (For interpretation of the references to colour in this figure legend, the reader is referred to the web version of this article.)

$$f_{\mathrm{b}_{0\circ}}(\gamma) = \frac{1}{6}\left(f_{\mathrm{q}_{1\circ}}\left(\gamma - \frac{1}{2}\right) + 4 f_{\mathrm{q}_{0\circ}}(\gamma) + f_{\mathrm{q}_{1\circ}}(\gamma)\right), \tag{12}$$

$$\begin{aligned}&f_{\mathrm{b}_{1\circ}}(\gamma) = \frac{2}{3} f_{\mathrm{q}_{0\circ}}(\gamma) + \frac{1}{3} f_{\mathrm{q}_{1\circ}}(\gamma), \\ &f_{\mathrm{b}_{2\circ}}(\gamma) = f_{\mathrm{q}_{1\circ}}(\gamma), \qquad f_{\mathrm{b}_{3\circ}}(\gamma) = f_{\mathrm{q}_{2\circ}}(\gamma), \\ &f_{\mathrm{b}_{4\circ}}(\gamma) = f_{\mathrm{q}_{3\circ}}(\gamma).\end{aligned} \tag{13}$$

Then

$$\begin{aligned}\mathrm{p}_0 &\overset{(10)}{=} \mathrm{avg}_\gamma(f_{\mathrm{b}_{1\circ}}(\gamma)) \\ &\overset{(12)}{=} \frac{2}{3} f_{\mathrm{q}_{0\circ}}(\gamma) + \frac{1}{3}\,\mathrm{avg}_\gamma(f_{\mathrm{q}_{1\circ}}(\gamma))\end{aligned} \tag{14}$$

and

$$\begin{aligned}f_{\mathrm{b}_{1\circ}}(\gamma) &\underset{(13)}{\overset{(12)}{=}} \frac{2}{3} f_{\mathrm{q}_{0\circ}}(\gamma) + \frac{1}{3} f_{\mathrm{b}_{2\circ}}(\gamma) \\ &\underset{(11)}{\overset{(10)}{\Rightarrow}} \mathrm{p}_0 + \frac{1}{3}(\mathrm{p}_1 c_\gamma + \mathrm{p}_2 s_\gamma) = \frac{2}{3} f_{\mathrm{q}_{0\circ}}(\gamma) \\ &\quad + \frac{1}{3}\left(\mathrm{p}_0 + \mathrm{p}_1 c_\gamma + \mathrm{p}_2 s_\gamma + \frac{2}{3}\mathrm{p}_3\right) \\ &\Rightarrow \mathrm{p}_3 = 3(\mathrm{p}_0 - f_{\mathrm{q}_{0\circ}}(\gamma)) \overset{(14)}{=} -f_{\mathrm{q}_{0\circ}}(\gamma) + \mathrm{avg}_\gamma(f_{\mathrm{q}_{1\circ}}(\gamma)).\end{aligned}$$

This yields the choice of p_0 and p_3 in (5).

9. The relation of polar splines to subdivision

A 2-layer polar configuration can be directly converted into a C^1 bi-3 spline cap such that $\mathbf{p}_1$ and $\mathbf{p}_2$ span the tangent plane at the pole $\mathbf{p}_0$. We use this fact to illustrate the relation of polar splines to subdivision. Improving on [16], this C^1 construction does not require an initial subdivision of the polar configuration: it yields equally good shape with fewer control points since $\mathbf{p}_k$ are derived using the knot-insertion analogy in Section 8.

Lemma 1. *The bi-3 spline with knots* $[0,0,0,0,1,2,3,4,5]$ *in the radial and* $\frac{1}{n}\mathbb{Z}_n$ *in the periodic direction and control points* $(\bar{\mathbf{b}}_{ij})_{i\in\{0,1,\ldots,4\},j\in\mathbb{Z}_n}$ *(cf. Fig. 8),*

$$\begin{aligned}&\bar{\mathrm{b}}_{0\circ} := \mathrm{p}_0\mathbf{1} \\ &\bar{\mathrm{b}}_{1\circ} := \mathrm{p}_0\mathbf{1} + \frac{1}{3}(\mathrm{p}_1\bar{\mathrm{v}}_1 + \mathrm{p}_2\bar{\mathrm{v}}_2) \\ &\bar{\mathrm{b}}_{i\circ} := \mathrm{q}_{i-1,\circ} \quad \textit{for } i \in \{2,3,4\},\end{aligned} \tag{15}$$

forms a C^1 *surface with bounded curvature, unless the* $\bar{\mathrm{b}}_{ij}$ *are in special position.*

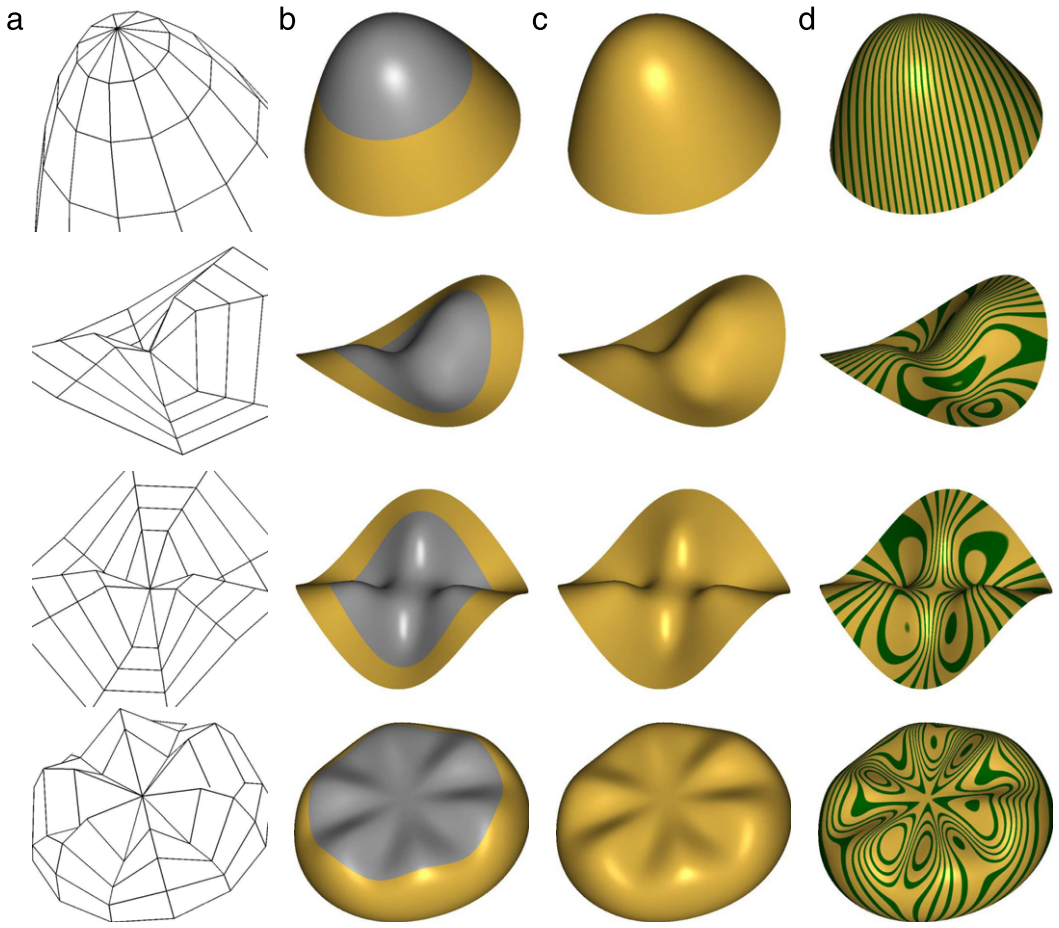

Fig. 9. Shape trials. (a) Each embedded polar configuration defines (b) a C^2 polar spline of degree (3, 6) (*gray*) surrounded by a bicubic spline ring (*gold*); (c) shows the ensemble. (d) Highlight lines show smoothness of the transition from the bicubic neighborhood to the pole. (For interpretation of the references to colour in this figure legend, the reader is referred to the web version of this article.)

Excluding control nets in 'special position' avoids discussing degenerate embeddings. The proof of tangent continuity and bounded curvature at the pole is identical to that in [16] since the 1-link $\overline{\mathtt{b}}_{1\circ}$ lies in *oval position*, i.e. satisfies for some point $\mathtt{o}$ and vectors $\mathtt{e}_1, \mathtt{e}_2$,

$$\overline{\mathtt{b}}_{1j} = \mathtt{o} + \mathtt{e}_1 c_{j/n} + \mathtt{e}_2 s_{j/n}, \quad c_{j/n} := \cos\frac{2\pi j}{n}.$$

Proof. We interpret $\overline{\mathtt{b}}$ as a polar subdivision control mesh, enumerated as a column vector, and devise a subdivision matrix $\overline{A}$ which composes the effect of

(i) inserting knots along the radial direction at the half integers, so that the radial knot sequence [0, 0, 0, 0, 1, 2, 3, 4, 5] is transformed to $\frac{1}{2}$[0, 0, 0, 0, 1, 2, 3, 4, 5]; and
(ii) projecting the 1-link into oval position.

Once the 1-link is in oval position, Step 2 above has no impact since radial knot insertion preserves the oval position. Essentially, $\overline{A\mathtt{b}} \in \mathcal{S}_3$ reparameterizes $h_{\overline{\mathtt{b}}}$ so that $h_{\overline{\mathtt{b}}}(\frac{1}{2}r, \gamma) = h_{\overline{A\mathtt{b}}}(r, \gamma)$. Spectral analysis of this subdivision algorithm then establishes bounded curvature at the pole $h_{\overline{\mathtt{b}}}(0, \gamma)$. □

A similar auxiliary C^2 subdivision algorithm can be defined to yield the C^2 polar spline $h_{\mathtt{b}}$. Its matrix A inserts knots in the radial direction and projects the resulting 1- and 2-links to satisfy the relationships (6). Spectral analysis of A yields the dominant six eigenvalues $(\lambda_0, \lambda_1, \lambda_2, \lambda_3, \lambda_4, \lambda_5) := (1, \lambda, \lambda, \lambda^2, \lambda^2, \lambda^2)$ where $\lambda := \frac{1}{2}$. The corresponding eigenvectors $\mathtt{w}_k$, $k \in \{0, \ldots, 5\}$, are

$$(\mathtt{w}_k)_{ij} := (\mathtt{u}_k)_i (\mathtt{v}_k)_j, \quad i \in \{0, \ldots, 6\}, j \in \{0, \ldots, 4n\} \tag{16}$$

($\mathtt{u}_k$ from (8) and $\mathtt{v}_k$ from (4)). As shown in Table 1, the corresponding splines satisfy the C^2 conditions in Theorem 7.16 of [17]

$$\{h_{\mathtt{w}_3}, h_{\mathtt{w}_4}, h_{\mathtt{w}_5}\} \in \operatorname{span}\{h^2_{\mathtt{w}_1}, h^2_{\mathtt{w}_2}, h_{\mathtt{w}_1} h_{\mathtt{w}_2}\}. \tag{17}$$

An alternative interpretation of our choice of $\mathtt{w}_k$ is therefore that we construct the spline so that its associated subdivision algorithm matches the C^2 conditions.

Conversely, subdivision theory prescribes a minimal generic degree of the C^2 polar spline (see Section 3 and Fig. 4): since C^2 continuity in the periodic direction requires periodic degree at least 3, $h_{\mathtt{w}_1}$ and $h_{\mathtt{w}_2}$ must have degree at least (1, 3) and, by (17), the degree is at least (2, 6) for $h_{\mathtt{w}_3}$, $h_{\mathtt{w}_4}$, and $h_{\mathtt{w}_5}$. To model higher-order (monkey) saddles, radial degree 3 is needed. In that sense, our degree (3, 6) is optimal.

10. Results and discussion

The test cases Figs. 9 and 10 illustrate the shape properties of C^2 polar splines over the first few modes of oscillation. We would like the surface to have low fluctuations in the distribution of Gaussian curvature and of the highlight lines; and it should continue the shape (curvatures) from the boundary data without abrupt changes. The comparison in Fig. 10 shows that a C^2 polar spline cap behaves qualitatively no different from its subdivision counterparts [14,16] even though it consists of just one spline patch.

To illustrate that C^2 polar splines are *bi*-3 C^2 *compatible*, Fig. 11 shows the interplay between regions defined by standard C^2 bi-3 tensor-product splines (gold in (c)), polar splines (grey in (c)),

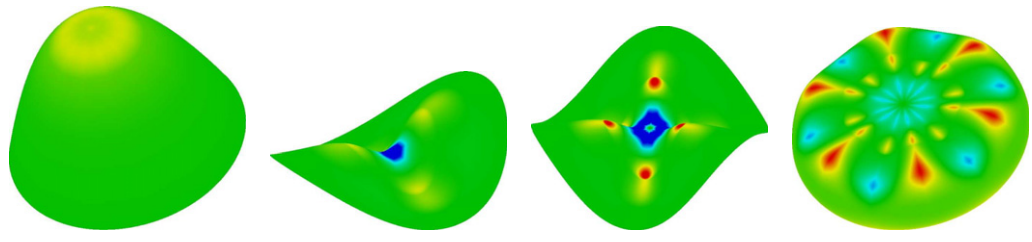

(a) (5, 6) Jet subdivision [KMP06].

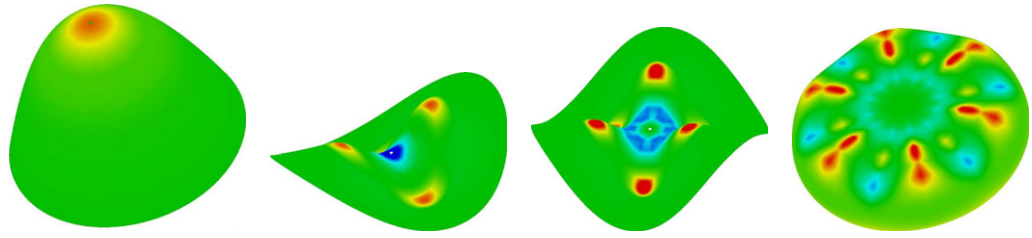

(b) (3, 3) subdivision [MKP08].

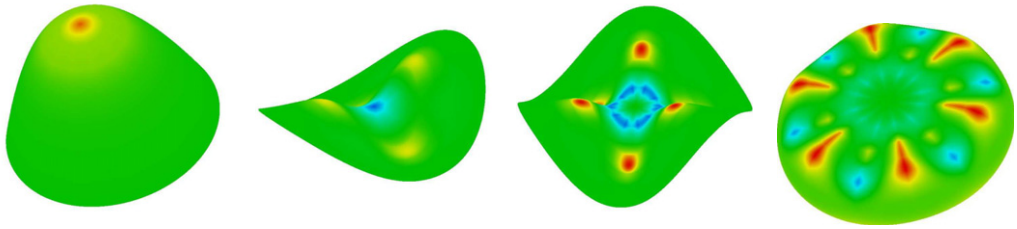

(c) Our single (3, 6) spline.

Fig. 10. Curvature comparison of C^2 Polar Jet Subdivision [14], Bi-3 C^2 Polar Subdivision [16], and our method. The Gauss curvature ranges from *blue* (negative) to *green* (near 0) to *red* (positive). (For interpretation of the references to colour in this figure legend, the reader is referred to the web version of this article.)

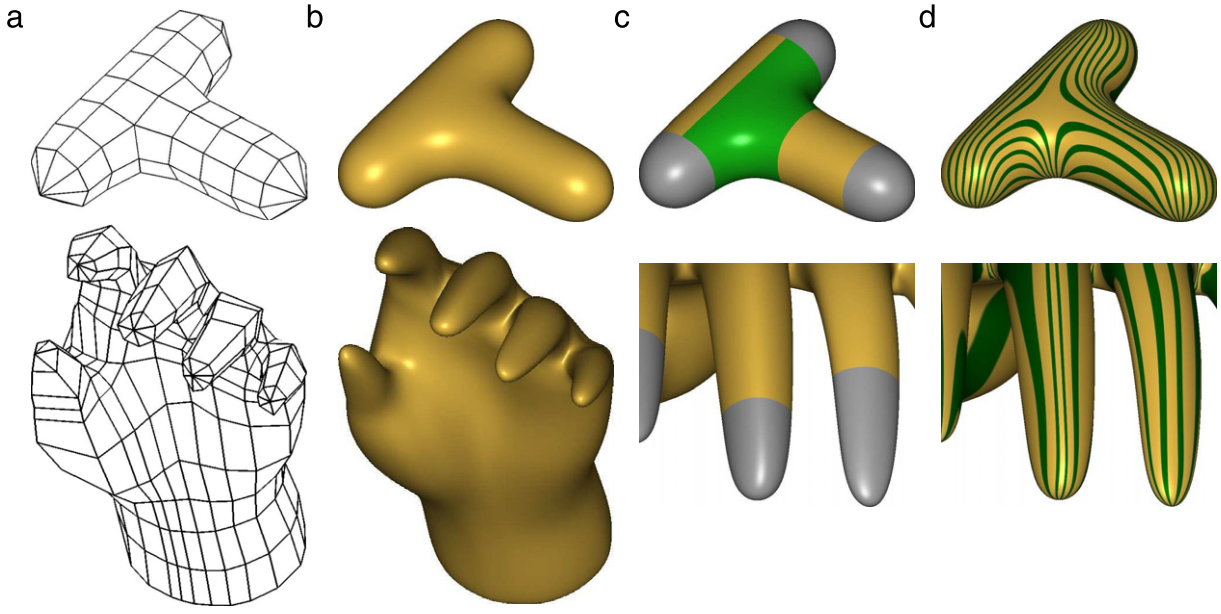

Fig. 11. The "Tee" and finger tips. (a) A quad mesh with polar configurations defines (b) the spline surface consisting of (c) uniform bicubics (*gold*), C^2 polar splines (*gray*), and bi-3 compatible schemes like [3,7,5] (*green*) that fill holes caused by extraordinary vertices. (d) The highlight lines flow smoothly across poles and the boundary of the polar spline. (For interpretation of the references to colour in this figure legend, the reader is referred to the web version of this article.)

and regions covered with a hole filling algorithm for extraordinary vertices (green in (c)). The Tee in Fig. 11 and the Chair in Fig. 2 have Catmull–Clark extraordinary vertices in the 3-link of a polar vertex so that the output of a bi-3 compatible algorithm

joins directly with the polar spline. While it is possible to adapt C^2 polar splines to allow for extraordinary vertices in the 2-link, it is preferable to have the designer introduce a separating edge-loop to unambiguously define the C^2 bi-3 transition between polar splines and bi-3 C^2 compatible splines. This also avoids having to modify existing algorithms [3–5] that expect a full quad neighborhood around extraordinary vertices.

The coefficients $\mathbf{p}_k$ correspond to intuitive geometric properties of the surface illustrated in Fig. 3. They can be adjusted by the user via the polar configuration control points or even directly to meet design constraints — without affecting the smoothness of the resulting spline surface.

To generalize the approach of this paper to C^K surfaces of degree $(K+1, K(K+1))$ at the pole, we need only choose functions h_{w_k} that span the Kth order Taylor expansion. The quality of the construction will then depend on the choice of coefficients $\mathbf{p}_k$.

Acknowledgment

This work was supported by the National Science Foundation Grant 0728797.

Appendix A. Multiplying uniform cubic splines

The product of two uniform cubics is a sextic spline with 4-fold knots. To form the product, we convert the cubics to Bézier form, multiply, and remove two knots at every breakpoint of the resulting spline of degree 6.

(i) A uniform spline with control points $[a_0, a_1, a_2, a_3]$ has Bézier control points

$$\frac{1}{6}[a_0 + 4a_1 + a_2,\ 4a_1 + 2a_2,\ 2a_1 + 4a_2,\ a_1 + 4a_2 + a_3].$$

(ii) Multiplying a pair of cubic polynomials with Bézier control points $[b_0, b_1, b_2, b_3]$ and $[\hat{b}_0, \hat{b}_1, \hat{b}_2, \hat{b}_3]$ yields degree 6 control points $c := [b_0\hat{b}_0,\ \frac{1}{2}b_0\hat{b}_1 + \frac{1}{2}b_1\hat{b}_0,\ \frac{1}{5}b_0\hat{b}_2 + \frac{3}{5}b_1\hat{b}_1 + \frac{1}{5}b_2\hat{b}_0,\ \frac{1}{20}b_0\hat{b}_3 + \frac{9}{20}b_1\hat{b}_2 + \frac{9}{20}b_2\hat{b}_1 + \frac{1}{20}b_3\hat{b}_0,\ \frac{1}{5}b_1\hat{b}_3 + \frac{3}{5}b_2\hat{b}_2 + \frac{1}{5}b_3\hat{b}_1,\ \frac{1}{2}b_2\hat{b}_3 + \frac{1}{2}b_3\hat{b}_2,\ b_3\hat{b}_3]$.

(iii) Two knots are removed from both ends of the degree-6 Bézier form to obtain the C^2 spline of degree 6 by the following sequence of operations ($\leftarrow$ indicates assignment).

remove knots once

$$c_0 \leftarrow 2c_0 - c_1, \qquad c_6 \leftarrow 2c_6 - c_5$$

remove knots again

$$c_1 \leftarrow 2c_1 - c_2, \qquad c_5 \leftarrow 2c_5 - c_4$$
$$c_0 \leftarrow 2c_0 - c_1, \qquad c_6 \leftarrow 2c_6 - c_5.$$

Combining these three steps, an explicit formula was derived and is implemented by the following C++ procedure.

```
// Multiply two uniform periodic degree 3 splines with
// n control points each to yield a single degree 6 spline
// with 4n control points and 4-fold knot multiplicity.
template <typename T1, typename T2>
void bsp_mul33(int n, const T1 a[], const T2 b[], T1 c[])
{
  for (int i = 0; i < n; ++i) {
    int im1 = (i-1+n)%n;
    int ip1 = (i+1)%n;
    int ip2 = (i+2)%n;
    const T1 &a0 = a[im1]; const T1 &a1 = a[i  ];
    const T1 &a2 = a[ip1]; const T1 &a3 = a[ip2];
    const T2 &b0 = b[im1]; const T2 &b1 = b[i  ];
    const T2 &b2 = b[ip1]; const T2 &b3 = b[ip2];
    c[4*i+0] = a0*b1/10.0 + a0*b2/30.0 + a1*b0/10.0
             + 8.0/15.0*a1*b1 + a1*b2/10.0
             + a2*b0/30.0 + a2*b1/10.0;
    c[4*i+1] = a0*b1/90.0 + a0*b2/45.0 + 16.0/45.0*a1*b1
             + 7.0/30.0*a1*b2 + 7.0/30.0*a2*b1
             + a2*b2/9.0 + a1*b0/90.0 + a2*b0/45.0;
    c[4*i+2] = a0*b3/720.0 + a1*b3/180.0 + a2*b3/720.0
             + a0*b1/720.0 + a0*b2/180.0 + a1*b0/720.0
             + 19.0/90.0*a1*b1 + 197.0/720.0*a1*b2
             + a2*b0/180.0 + 197.0/720.0*a2*b1
             + 19.0/90.0*a2*b2 + a3*b0/720.0
             + a3*b1/180.0 + a3*b2/720.0;
    c[4*i+3] = a1*b1/9.0 + 7.0/30.0*a1*b2 + a1*b3/45.0
             + 7.0/30.0*a2*b1 + 16.0/45.0*a2*b2
             + a2*b3/90.0 + a3*b1/45.0 + a3*b2/90.0;
  }
}
```

Appendix B. Masks for Step 0

Step 0 of the a C^2 polar spline construction (Fig. 6) refines the polar configuration according to [16], i.e. with the masks of Fig. B.1 and

$$\alpha := \beta - \frac{1}{4}, \qquad \beta := \frac{5}{8}, \qquad c_\gamma := \cos(2\pi\gamma),$$
$$\gamma_k := \frac{1}{n}\left(\beta - \frac{1}{2} + \frac{5}{8}c_{k/n} + (c_{k/n})^2 + \frac{1}{2}(c_{k/n})^3\right).$$

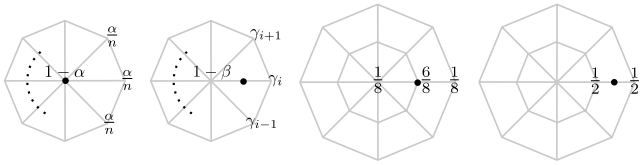

Fig. B.1. Refinement rules for Step 0 (from [16]).

References

[1] Karčiauskas K, Peters J. Surfaces with polar structure. Computing 2007; 79(March):309–15.
[2] Myles A, Peters J. Bi-3 C^2 polar subdivision. ACM Trans Graph 2009;28(3):1–12.
[3] Prautzsch H. Freeform splines. Comput Aided Geom Des 1997;14(3):201–6.
[4] Karčiauskas K, Peters J. Guided spline surfaces. Comput Aided Geom Des 2009; 26(1):105–16.
[5] Loop CT, Schaefer S. G^2 tensor product splines over extraordinary vertices. In: Computer graphics forum (proceedings of 2008 symposium on geometry processing) 27, 5, 2008. p. 1373–82.
[6] Reif U. TURBS—topologically unrestricted rational B-splines. Constructive approximation. Int J Approx Expansions 1998;14(1):57–77.
[7] Peters J. C^2 free-form surfaces of degree (3, 5). Comput Aided Geom Des 2002; 19(2):113–26.
[8] Ying L, Zorin D. A simple manifold-based construction of surfaces of arbitrary smoothness. ACM Trans Graph 2004;23(3):271–5.
[9] Levin A. Modified subdivision surfaces with continuous curvature. In: SIGGRAPH '06: ACM SIGGRAPH 2006 papers. New York (NY, USA): ACM Press; 2006. p. 1035–40.
[10] Karčiauskas K, Peters J. Concentric tessellation maps and curvature continuous guided surfaces. Comput Aided Geom Des 2007;24(2):99–111.
[11] Loop CT. Second order smoothness over extraordinary vertices. In: Symposium on geometry processing. New York (NY, USA): ACM; 2004. p. 165–74.
[12] Bohl H, Reif U. Degenerate Beźier patches with continuous curvature. Comput Aided Geom Des 1997;14(8):749–61.
[13] Zorin D. Constructing curvature-continuous surfaces by blending. In: Symposium on geometry processing. Eurographics Association; 2006. p. 31–40.
[14] Karčiauskas K, Myles A, Peters J. A C^2 polar jet subdivision. In: Symposium on geometry processing. Eurographics Association; 2006. p. 173–80.
[15] Karčiauskas K, Peters J. Finite curvature continuous polar patchworks. In: Hancock E, Martin RR, Sabin M, editors. IMA Mathematics of Surfaces XIII Conference. 2009. p. 222–34.
[16] Myles A, Karčiauskas K, Peters J. Pairs of bi-cubic surface constructions supporting polar connectivity. Comput Aided Geom Des 2008;25(8):621–30.
[17] Peters J, Reif U. Subdivision surfaces. Geometry and computing, vol. 3. New York (NY, USA): Springer-Verlag, New York, Inc.; 2008.